Broadband microseismic observations from a Montney hydraulic fracture treatment, northeastern B.C., Canada

David Eaton[1], Mirko van der Baan[2], Jean-Baptiste Tary[2], Brad Birkelo[3], Neil Spriggs[4], Sarah Cutten[5] and Kimberly Pike[1]

[1]Department of Geoscience, University of Calgary, Calgary, Alberta, Canada; [2]Department of Physics, University of Alberta, Edmonton, Alberta, Canada; [3]Spectraseis Inc.; [4]Nanometrics Inc.; [5]ARC Resources Ltd., Calgary, Alberta, Canada

Summary

A research project was undertaken in August 2011 for continuous passive monitoring of a multistage hydraulic fracture stimulation of a Montney gas reservoir near Dawson Creek, B.C., with the main objective of investigating low-frequency characteristics of microseismic events. This work was motivated by a recently discovered class of long-period long-duration (LPLD) events, interpreted to represent slow slip along pre-existing fractures. The field deployment included a 6-level downhole toolstring with low-frequency (4.5 Hz) geophones and a set of 21 portable broadband seismograph systems. Time-frequency analysis of extracted high- and low-frequency microseismic events made use of the short-time Fourier transform. Observed low-frequency microseismic signals included tremor phenomena at various time scales, from a few seconds to the entire duration of high-pressure fluid injection, in addition to inferred regional earthquakes located ~150 km from the monitoring site. Relative to previously documented LPLD events from the Barnett, differences in low-frequency response for this Montney stimulation are interpreted to reflect a lower degree of complexity of pre-existing and induced fracture networks. Analysis of low-frequency microseismic signals shows promise for improving geomechanical understanding of fracture processes.

Introduction

In recent years, seismologists have increasingly recognized the significance of low-frequency earthquakes. Terms such as non-volcanic tremor and slow-slip earthquakes are often applied to describe this phenomenon, which constitutes a significant component of the spectrum of energy radiated from earthquake fault systems (Beroza and Ide, 2011). Das and Zoback (2011) recently documented a new class of frac-induced microseismicity, long-period long-duration (LPLD) events, that have similar characteristics to some classes of low-frequency seismic activity. LPLD events are distinguished from conventional high-frequency microseismic events by their relatively low frequencies (10-80 Hz), long durations of 20-50 s, and some waveform characteristics similar to tectonic tremor in fault systems. By analogy with tremor-like phenomena observed in a variety of fault systems (e.g. Shelly et al., 2007), Das and Zoback (2011) interpreted these signals as slow slip activated on pre-existing fracture systems by the hydraulic fracture treatment.

With these considerations in mind, a research project to acquire microseismic data was undertaken August 7-29, 2011 near Dawson Creek, B.C. Named the Rolla Microseismic Experiment (RME), this work involved recording of several multistage hydraulic fracture treatment programs performed in two horizontal wells (Figure 1). The microseismic data were collected using both surface and borehole sensors. The borehole toolstring consisted of a 6-level low-frequency system with downhole digitization. Surface sensors included a 12-channel array with a mix of vertical-component and 3-C geophones, and 22 broadband sensors (Trillium Compact seismometers and Taurus digitizers) deployed in 7 localized arrays over an area of ~ 0.5 km2. Data acquisition parameters are summarized in Table 1.

The unusual setup was employed to investigate multiple objectives. First, microseismic monitoring was performed using both surface and borehole equipment to compare both acquisition strategies in order to determine their mutual advantages and inconveniences such as ease of deployment, costs, detectability of events, other signals and associated noise levels. The experiment was also unusual in that both broadband and short-period equipment was deployed. The approximate lowest recording frequencies for the various sensors are: broadband surface-based seismometers, 0.0083 Hz (= 120 s); borehole equipment, 0.1 Hz; short-period surface array, 5 Hz. Data analysis of the variously recorded signals thus helps to reveal if significant energy is present below the low-frequency limit (~ 10 Hz) imposed by most standard monitoring equipment. It also may obscure proper identification of so-called slow earthquakes (Ide et al., 2007) occurring on much longer time scales than conventional earthquakes resulting from abrupt brittle failure.

Table 1: Summary of data-acquisition parameters.

Manufacturer	Type of Sensor	Number of Sensors	Sample Rate (ms)	Start/End Dates	Sensor Spacing
Spectraseis	4.5 Hz 3C geophones	6	0.5	Aug. 15-18 and Aug. 21-25	32 m (borehole)
Nanometrics	Broadband seismometer (Trillium Compact)	21	2.0	~ Aug. 8 to Aug. 27	50 m (4-element surface array)
ESG	10 Hz geophones (mix of Z and 3C)[1]	8	0.5	Aug. 15-18	20 m (8-element surface array)

[1] *Data from the surface geophone array are not used in this paper.*

Broadband microseismic observations...

In this paper, we first describe the geological setting and operational setup for the RME. Next we outline the results from conventional microseismic analysis of the downhole observations, which focus on high-frequency microseismic events. We then undertake time-frequency analysis of the continuous datastream using short-time Fourier transforms to examine variations in local frequency content and highlight slow-deformation processes. This approach is motivated by similar analysis of acoustic emissions generated during laboratory rock-fracturing experiments, which have greatly aided in improving our understanding of active microcracking and deformation processes (Benson et al., 2008; Thompson et al., 2009).

Geological Setting and Operational Setup

Significant gas reserves are hosted by the Triassic Montney Formation in northeastern British Columbia and northwestern Alberta. Although estimates of natural gas in place are highly variable, ranging from 80 to 700 Tcf, in recent years production has increased dramatically to over 400MMcf/d (Walsh et al., 2006). The Montney Formation is an extensive siliciclastic-dominant unit that occurs from west-central Alberta to northeast British Columbia (Dixon, 2000); in the area of this study, it is overlain by the Triassic Doig Formation and underlain by the Permian Belloy Formation. The depositional environment of the Montney ranges from shallow-water shoreface sands to offshore marine muds (NEB, 2009). The reservoir rocks consist of interbedded shale, siltstone and sandstone layers, dominated by shale and silty shale (Dixon, 2000). Thickness can range up to 300m, while porosity is very low, ranging from 1.0-6.0% (NEB, 2009).

The overall layout of field equipment and relative location of the two treatment wells (A and B) are shown in Figure 1. The 10-stage fracture treatment program in well A took place August 15-18 and the 11-stage treatment program in well B took place August 21-25. Layout of the field equipment commenced

August 8, and continuous recordings using surface sensors commenced prior to the start of the first stage of hydraulic fracturing. The broadband seismograph units recorded data continuously until August 27, whereas the surface geophone array was decommissioned on August 18 and thus only recorded the 10-stage frac treatment in well A.

The six borehole array sondes were deployed on production tubing in the deviated monitor well (Figure 2). The geophone sondes were located a few hundred m above the reservoir unit, and coupling of the sondes to the wellbore casing was achieved by setting the tubing down on a packer. The total vertical aperture of the array was 160m. The array was retrieved and the data downloaded between the hydraulic fracture treatment programs in wells A and B, and again after completion of the well B treatment.

Analysis of high-frequency signals

Data recorded using the downhole arrays were processed using a workflow that included:

1. Instrument response correction to convert raw amplitudes to units of m/s;

2. Analysis of perforation shots to calibrate the background velocity model and determine sonde orientations for the two deployments;

3. Automatic event detection using an amplitude-based triggering algorithm;

4. Rotation of recorded signals from original orientations (axial plus two mutually perpendicular components in the plane locally perpendicular to the borehole) to fixed orientations (vertical, east-west, north-south);

5. Interactive picking of P- and S-arrivals plus event classification;

6. Determination of hypocentre locations using a least-squares algorithm;

7. Estimation of event magnitudes based on the Brune model.

Examples of waveforms recorded from perforation shots together with time-frequency analyses are shown in Figure 3. As
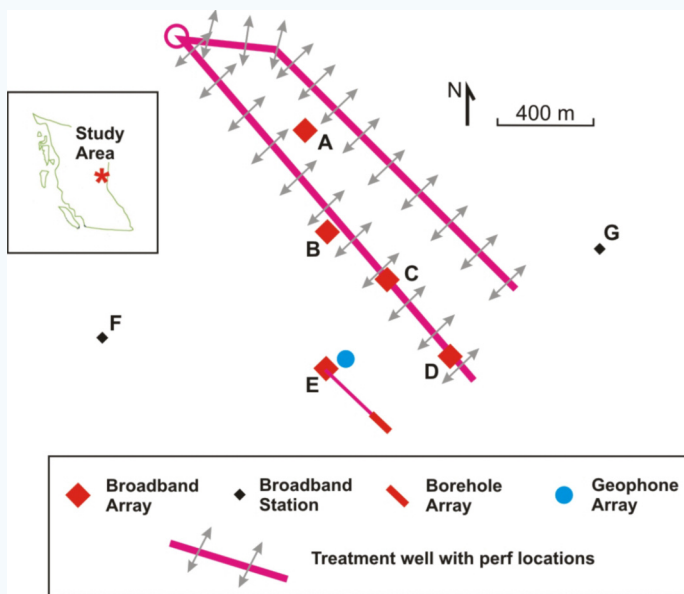

Figure 1. Overall layout of the Rolla Microseismic Experiment. Three types of microseismic recording systems were used: a borehole toolstring; a set of broadband seismograph systems deployed within four-station arrays or as individual stations; and a 12-channel array of geophones located near the borehole system.
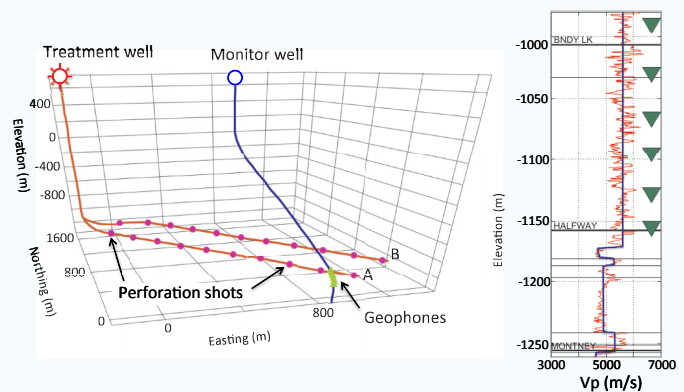

Figure 2. Left: Perspective view of the monitor and treatment wells. Right: P-wave velocity log showing formation tops, blocked velocity model and geophone depth locations (inverted triangles).

Broadband microseismic observations...

Continued from Page 45

expected due to the volumetric nature of explosive sources, the waveforms are dominated by the direct P-wave. It is also possible to discern S-wave arrivals, which is important for calibration of the velocity model. For the closest shot location (~350m), the data contain usable signal up to the Nyquist frequency (1 kHz). The high-frequency content diminishes with distance due to the effects of anelastic attenuation. Waveform examples of high-frequency microseismic events are presented in Figure 4. In this case, the S-wave arrival has the highest amplitudes. The frequency content of these signals is predominantly concentrated above 100 Hz, and the bandwidth decreases with distance due to the effects of attenuation.

Figure 5 shows the computed moment magnitude (*Mw*) for all detected events, plotted versus distance from the centroid of the downhole geophone array. Graphs such as these are useful QC tools to identify magnitude anomalies and to assess the magnitude detection threshold. The detection threshold is a function of distance and refers here to the magnitude above which detection probability is approximately 100%. It is obtained by solving

$$\frac{\omega R M_w}{4\pi\rho r V_S^3} \exp\left(-\frac{\omega r}{2 Q_S V_S}\right) = A_{max} \quad , \quad (1)$$

where $\omega = 2\pi f$ is angular frequency, $R = 0.63$ is the average radiation pattern for S waves (Boore and Boatwright, 1984), ρ is density, r is source-receiver distance in m, V_S is shear-wave velocity in m/s, Q_S is the shear-wave quality factor, and A_{max} is the maximum level of background noise in m/s. Here, detection limit refers to the magnitude below which detection probability is reduced to zero; the formula is similar to equation (1), except that A_{max} is replaced with A_{mix}, the minimum level of background noise. The parameters used here to evaluate detection threshold/limit are: $f = 200$ Hz, $V_S = 2500$ m/s, $\rho = 2500$ kg/m^3, $Q_S = 5000$, $A_{max} = 6.5 \ 10^{-9}$ m/s, $A_{max} = 3.25 \ 10^{-9}$ m/s.

Figure 6 shows a synoptic plot comparing recorded microseismic data over the duration of a treatment stage with pumping curves (downhole treatment pressure, blender density and slurry rate). The time series in this figure is constructed by combining positive values from high-pass filtered data (>200 Hz) with negative values from a low-pass filtered trace (< 50 Hz). The purpose of this is to highlight simultaneously both high-frequency and low-frequency responses. Also shown are detected high-frequency events (indicated by positive bars) and tube waves (indicated by negative bars). Some salient features of this plot are:Amplitude modulation of both high- and low-frequency microseismic data, evidenced by the envelope of the amplitude values, shows a trend that appears to correlate with the treatment pressure curve. For most other treatment stages, this amplitude modulation is more apparent for the low-frequency data. As discussed below, this phenomenon is interpreted as tremor associated with pumping noise generated at the treatment wellhead.
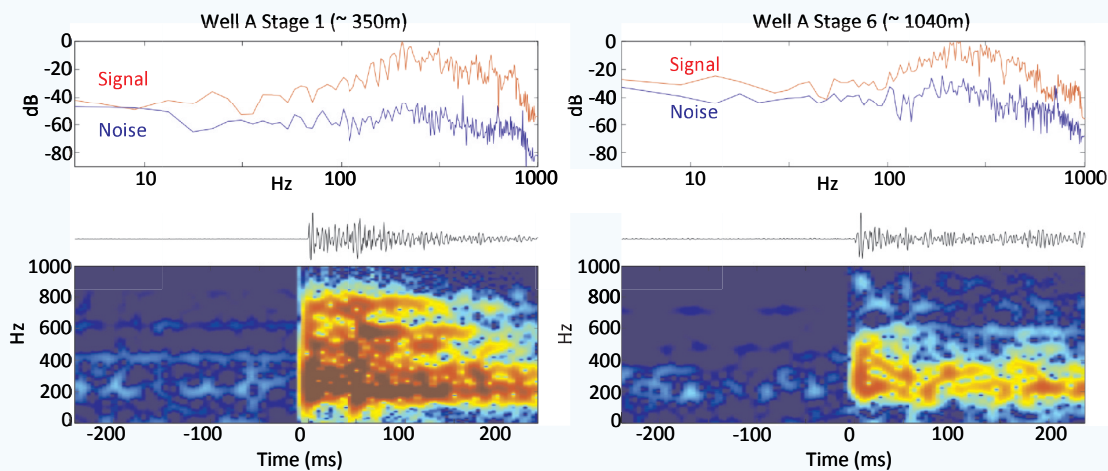

Figure 3. Examples of perforation shots, which are generally dominated by P arrivals. Upper panels: signal and noise spectra. Lower panels: recorded waveforms and their corresponding spectrograms obtained using the short-time Fourier transform.
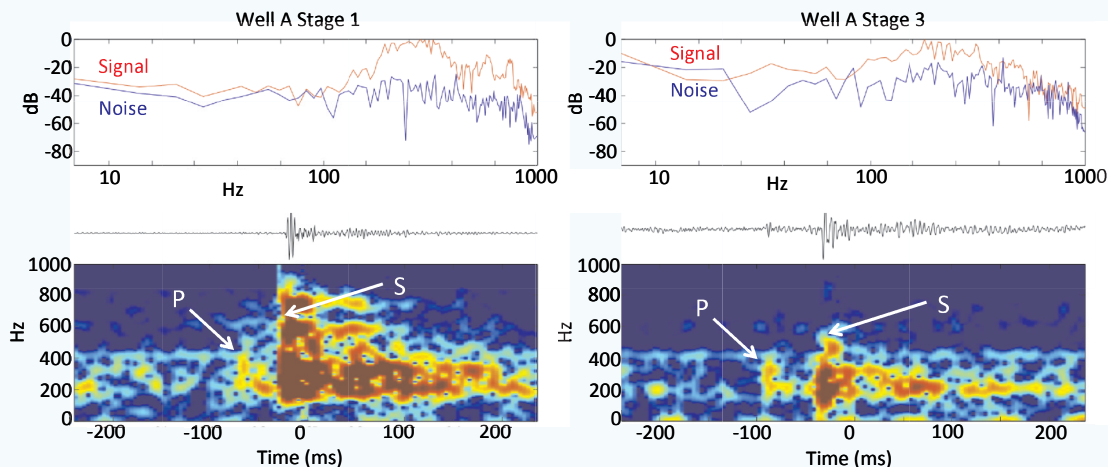

Figure 4. Examples of high-frequency microseismic events, which are generally dominated by S arrivals. Upper panels: signal and noise spectra. Lower panels: recorded waveforms and corresponding spectrograms obtained using the short-time Fourier transform.

Broadband microseismic observations...

1) Potential high-frequency events are marked by high-amplitude spikes in the high-pass filtered microseismic time series. Locatable events, where both P and S-wave arrivals are visible as shown in Figure 4, do not occur until the second half of the treatment stage with proppant levels are increased as indicated by the blender density (green curve in Figure 6).

2) Low-frequency events (LFE's) are marked by high-amplitude spikes in the low-pass filtered microseismic time series. In some cases these correlate with high-frequency events, and in other cases these correlate with tube-wave arrivals.

Analysis of low-frequency signals

A systematic search for low-frequency signals was carried out using an approach similar to steps 1, 3 and 4 in the high-frequency workflow. In this case, however, two low-pass filters were first applied to the data, with cutoff frequencies of 100 Hz and 25 Hz, respectively. All events that were detected with the 25 Hz cutoff but not with the 100 Hz cutoff were examined using a time-frequency analysis approach based on the short-time Fourier transform. This dual-detection approach was used to eliminate unnecessary analysis of high-frequency events that also contain significant signal content below 25 Hz. Due to the long duration of LPLD events, an initial long time window (~ 5 minutes) was used. The time window was then reduced, on a case-by-case basis. A total of 50 events were identified in this way, of which 24 are of long duration (> 20s) and the remaining are of shorter duration. The former is referred to here as long-duration low-frequency tremor, and the latter are referred to here as low-frequency events (LFE's). In addition, the envelope of the low-frequency signals (Figure 6) was investigated. Each of these types of low-frequency signals is considered separately in the following sections.

Figure 7 shows an example of a long-duration low-frequency tremor signal. Although this has some characteristics of LPLD events as described by Das and Zoback (2011), the frequency content is significantly lower (< 20 Hz). Figure 8 shows two examples of low-frequency events (LFE's) followed by subsequent

high-frequency events. This apparent causal relationship between these classes of microseismic activity occurs in about 20% of the cases examined.

Figure 9 shows an analysis of the average spectral content of vertical-component signals recorded on surface broadband seismograph stations (Figure 1) during and before the stage 3 hydraulic treatment in well A. The data recorded during the treatment contains spectral peaks centred at 5.5, 7.8 and 11.0 Hz, respectively. Although the spectral peak at 5.5 Hz may be related to background noise, the others are absent or significantly reduced for the non-frac time window, which is assumed to characterize
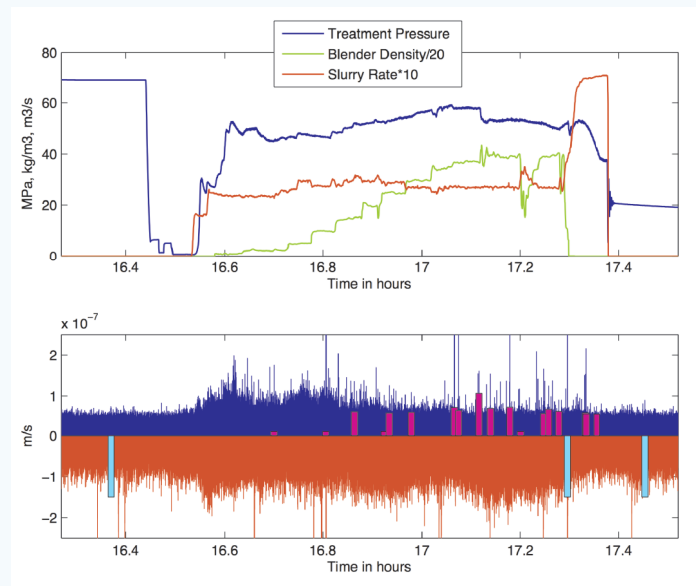

Figure 6. Synoptic plot comparing the recorded data (lower panel) from downhole geophone level 3 (vertical component) with pump curves from the A3 frac treatment. Time axis is Universal Time (UTC). The time series in the lower panel is constructed using negative values from the low-pass filtered seismic trace, multiplied by 10, and positive values from the high-pass filtered seismic trace. This time series highlights both high frequency events (shown as positive spikes) and low-frequency events (shown as negative spikes). Magenta and cyan bars indicate analyzed high-frequency events and tube waves, respectively.
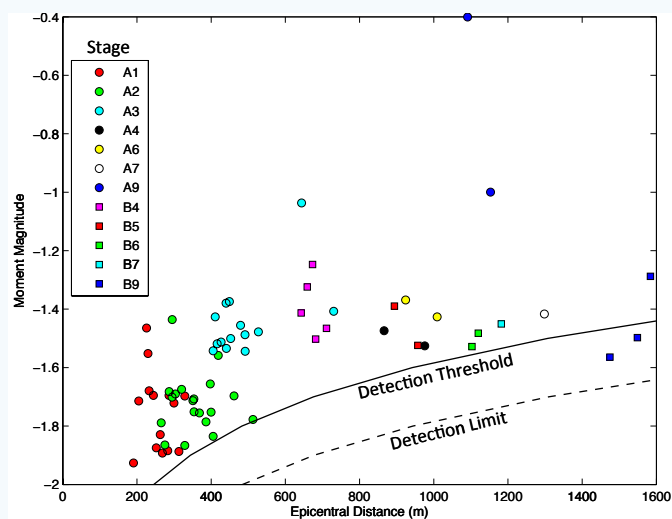

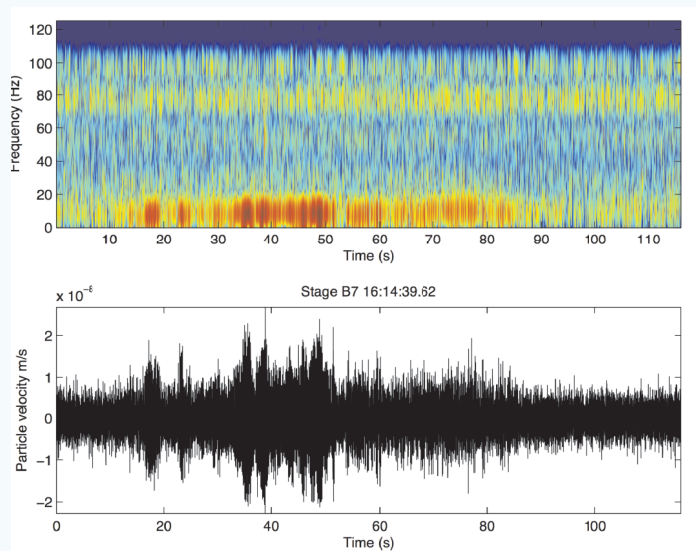*Figure 5. Magnitude-distance graph for all analyzed high-frequency microseismic events.*

Figure 7. Example long-duration low-frequency tremor.

Broadband microseismic observations...

the background noise levels. These peaks are most conspicuous for array A (located closest to the treatment well pad), less conspicuous for array B (located about 400 m south of array A), and virtually absent for the other arrays. This pattern suggests that the source of the spectral energy in this low-frequency band comprises pumping equipment associated with the hydraulic fracture stimulation.

In order to examine low-frequency tremor extending over the duration of the fracture treatment, we computed an amplitude envelope function for the continuous microseismic data using the following approach:

1. A low-pass filter was applied, with a cutoff frequency of 25 Hz.
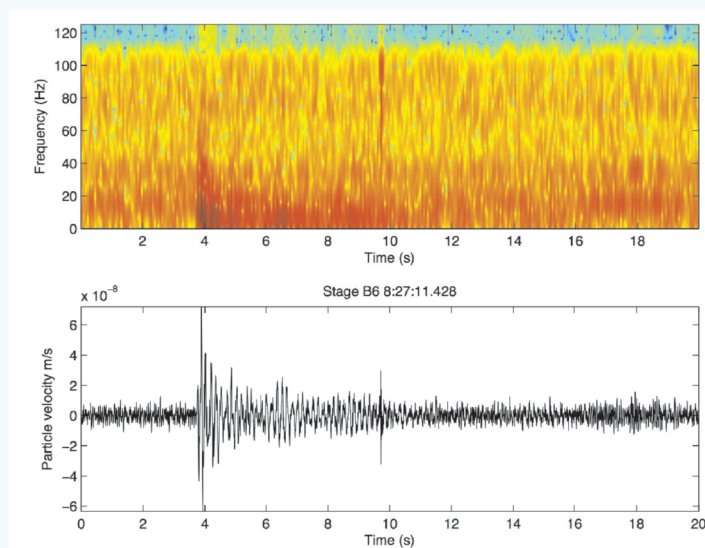
2. The absolute value of the data was computed.

3. A 5-s running median filter was applied to the rectified data to remove amplitude spikes.

Figure 10 shows the low-frequency tremor envelope computed in this fashion for treatment stages 1-8 of well A. Stages 9 and 10 are note considered here, as the data contain strong signals from teleseismic earthquakes that distort the calculations. To facilitate comparison, the envelope signals are aligned based on the start time of each stage. While details vary from stage-to-stage, this plot indicates that, for this low frequency band, long-duration tremor signals are characterized by similar amplitude levels for each stage. Since the distance from the monitor well increases from stage 1 to 8, this analysis suggests that (to first order) the signal does not vary with distance from the treatment location.

Figure 11 shows an enlargement of a representative short time window containing low-frequency tremor signals. The signals

Figure 8. Two examples of a low-frequency event followed by a high-frequency event.
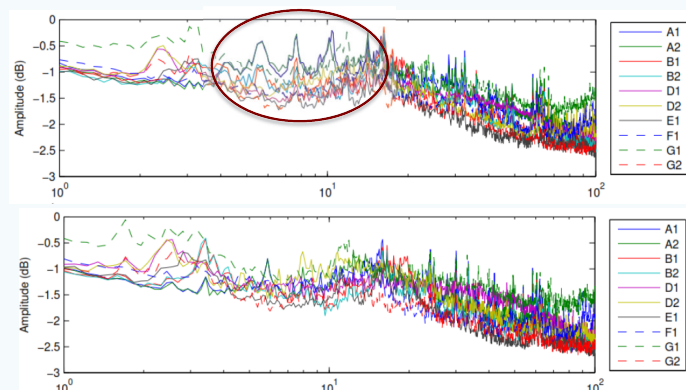

Figure 9. Fourier spectra computed using vertical-component recordings from surface seismographs (see Figure 1). Upper panel: spectra computed during the stage 3 treatment in well A. Lower panel: spectra computed while no hydraulic fracturing was taking place. Circled area shows spectral peaks at 5.5, 7.8 and 11.0 Hz (see text).
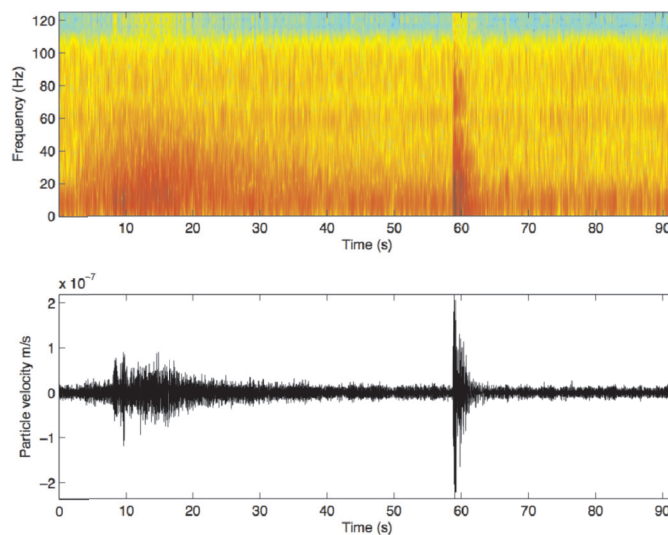

Figure 10. Tremor-envelope functions for treatment stages 1-8 of well A, aligned on the start time of each treatment stages. The overall similarity in amplitude of these functions suggests that the phenomenon does not depend on distance from the treatment stage. The arrow shows an inferred regional earthquake signals (see Figure 12).

Broadband microseismic observations…
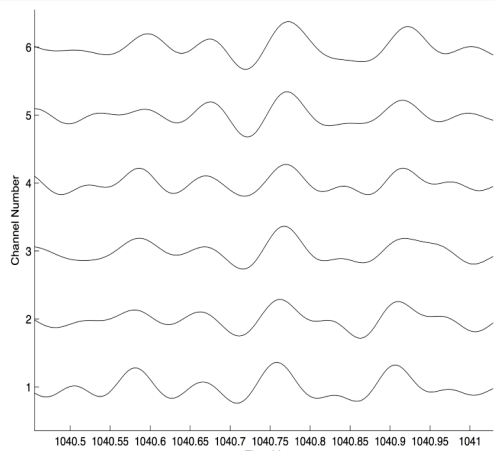
Continued from Page 48

Figure 11. Detail of tremor signals observed on vertical-component downhole geophones during treatment stage 3 of well B. The apparent velocity of these signals is 10.25 km/s.

occur predominantly on the vertical component, suggesting a dominantly vertical polarization direction. In addition, the apparent velocity of the signals is > 10 km/s. Taken together, these characteristics suggest that the tremor signals are comprised largely of near horizontally propagating S-waves.

It is important to distinguish between potential LPLD events associated to the hydraulic fracturing treatment and local earthquakes. For example, Fig 12 shows a number of recorded signals that are interpreted here as regional earthquakes that are unrelated to this hydraulic fracture treatment. When viewed using suitably long time windows, several of these events exhibit pairs of arrivals that are dominated by frequencies less than 20 Hz and separated by ~ 18s. If these represent direct P and S arrivals from an earthquake, this implies an epicentral distance of about 150 km, based on the velocity model used by the Alberta Geological Survey to determine earthquake locations (Virginia Stern, pers. comm., 2013):

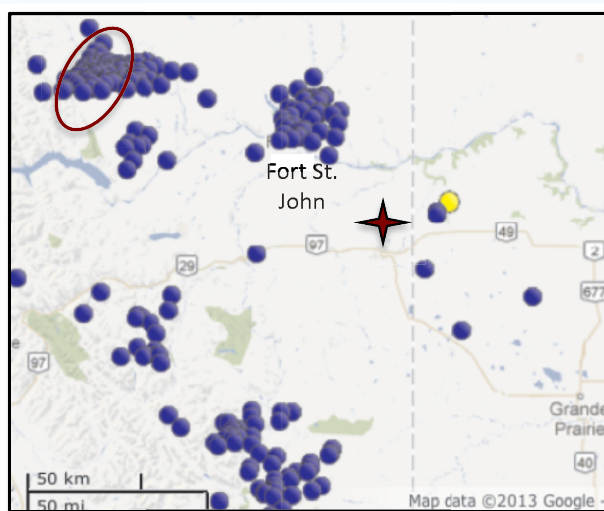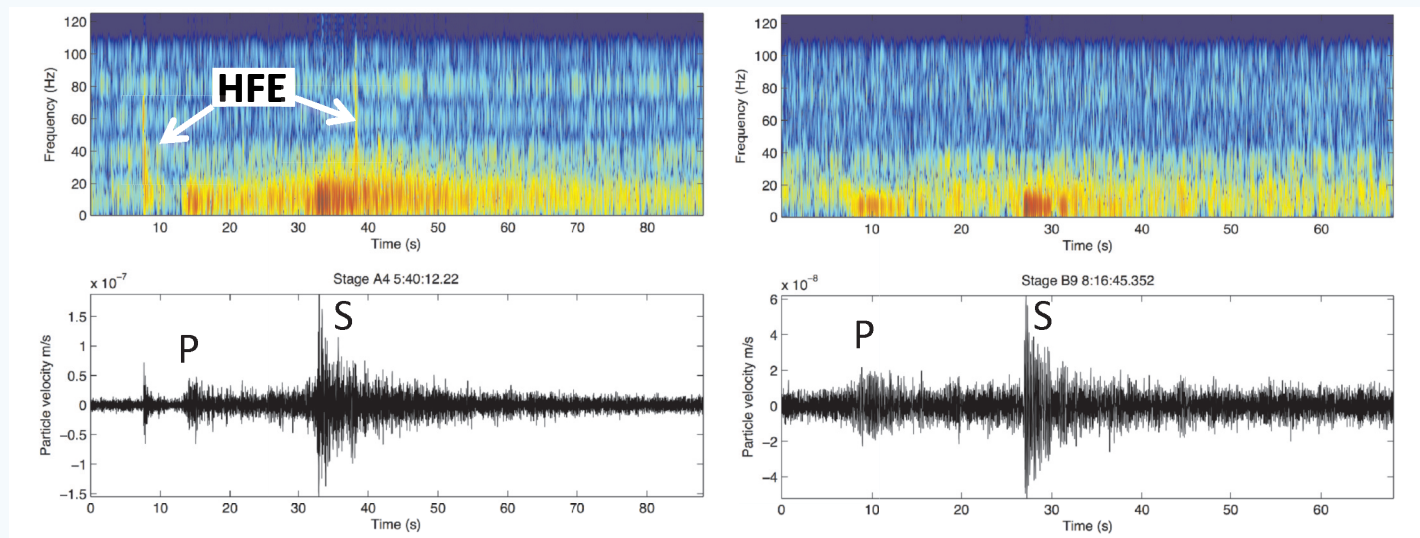| Depth	P	S
0-36	6.2 km/s	3.57 km/s
36	8.2 km/s	4.7 km/s

Figure 12. Examples of low-frequency signals that coincide with the hydraulic fracture treatment, yet are interpreted to arise from regional earthquakes. The example on the left also contains several high-frequency events that overlap in time with the low-frequency tremor. The S-P time difference (~ 18s) is consistent with an epicentral distance of ~150 km based on the velocity model used to locate earthquakes in Alberta. The lower panel shows earthquake events in the Canadian national earthquake catalog from 2000/01/01 to 2013/02/04. The estimated distance of 150 km correlates with a cluster of earthquakes west of Fort St. John, BC. Red star symbol shows approximate location of the RME.

Broadband microseismic observations...

Continued from Page 50

Assuming that this is an earthquake, Figure 12 shows a circle identifying possible locations of the epicenter. This circle encloses an earthquake-prone area west of Fort St. John. The event is thus interpreted as a natural seismic event, unrelated to this hydraulic fracture treatment, located about 150 km from the monitor well. No events from this region are listed during August 2011 in the GSC's online national earthquake catalog (http://www.earth-quakescanada.nrcan.gc.ca/stndon/NEDB-BNDS/bull-eng.php, accessed on 2013/02/01), suggesting that its magnitude is less than the detection threshold of M ~ 2.5 for the catalog.
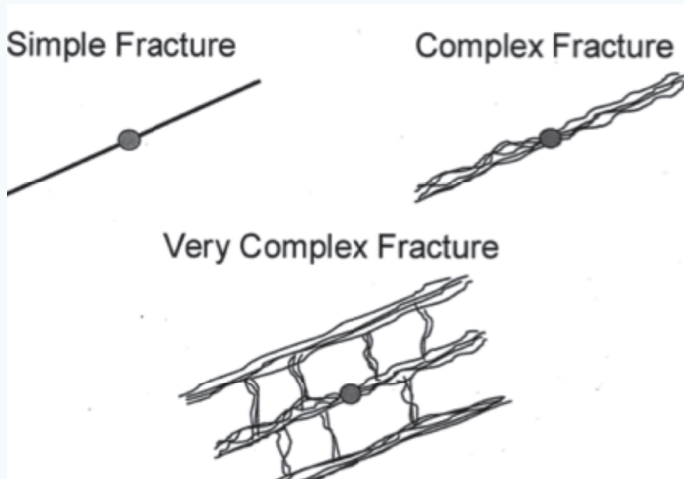

Figure 13. Illustration of hydraulic-fracture complexity, showing hierarchy of complexity in various U.S. unconventional gas plays (Fisher et al., 2005). The classical description of a simple fracture comprises a single-planar bi-wing crack. The presence of complex fracture networks, considered to be the case for the Barnett shale, is desirable for production. Observation of LPLD events in the Barnett shale but not in the Montney is inferred to reflect a higher level of fracture complexity in the Barnett.

Discussion

Based on our experience from western Canada, high-frequency microseismic events from this hydraulic-fracture stimulation program are sparse relative to other regions. In particular, it is not unusual to record > 100 events per treatment stage for the rate/volume/pressure parameters used here. Although the paucity of events may, in part, reflect the relatively large lateral separation of the monitor well from the treatment zones for this experiment (350-2000 m), we remark that perforation shots were well recorded to a distance of 2000m. Instead, we interpret much of the reduced high-frequency signals to a less brittle response to high-pressure fluid injection of the silty shale Montney reservoir unit in this region than for other unconventional reservoirs in western Canada.

Another noteworthy attribute of the high-frequency microseismicity is an apparent delayed onset of locatable events (i.e., events that contain clear P and S arrivals) until the proppant concentration, represented in Figure 6 by the blender density, achieves ~30% of its maximum value. Prior to this point in the treatment, deformation associated with tensile opening of the hydraulic fracture appears to produce fewer and weaker microseismic events. Under the prevailing geomechanical conditions for this treatment, this behavior may reflect a period of less brittle deformation that occurs before injection of proppant into the reservoir.

Although only 50 low-frequency events were detected during the stimulation programs, the signals documented here provide potential insights into fracturing processes. In particular, we interpret the low-frequency signals (tremor) to mark deformation processes that are otherwise aseismic. In addition, the precursory temporal relationship observed in some cases (Figure 8) suggests a possible causal relationship sometimes exists between tremor and subsequent high-frequency deformation processes.

It is also noteworthy that none of the low-frequency signals observed here strongly resemble LPLD events from the Barnett shale, which have frequencies of 5-50 Hz and durations of 30-50 s (Das and Zoback, 2011). In their interpretation, Das and Zoback (2011) suggested that LPLD events could represent slow slip on fracture zones near the treatment well. They also suggested that the abundance of LPLD events depends on the density of fractures in the treatment zone. The Barnett shale is noted for fracture-network complexity (Fig. 13; Maxwell et al., 2002). Thus, a possible source of the difference in low-frequency response between the Barnett shale and the Montney formation may stem from inherent differences in complexity of the pre-existing and induced fracture network.

During these hydraulic-fracture stimulation programs we observed tremor that persisted throughout the duration of the treatment stage. Surface observations using broadband seismograph equipment reveals discrete frequency bands of 5.5, 7.8 and 11.0 Hz, respectively during the treatment stage, with amplitude that diminishes with distance from the treatment well pad. These characteristics suggest that the low-frequency signals are generated by hydraulic-fracture pumping equipment used during the treatment. Similarly, downhole recordings reveal tremor signals within the same frequency range as the surface sensors. The downhole signals are most pronounced on the vertical component, and show an apparent velocity of ~ 10 km/s. The amplitude envelope of the tremor remains roughly constant for treatment stages at a range of distances from the monitor well. Taken together, we interpret these observations to originate from coupling of pump-generated vibrations into the subsurface through the treatment wellbore, which acts as a seismic line source. The downhole tremor observations are interpreted as diffuse wavefields composed of S waves that are scattered at geological contacts and/or within the treatment zone.

Conclusions

This study presents results from a research project that acquired continuous passive seismic recordings of a multistage hydraulic fracture treatment of a Montney reservoir in northeastern B.C. A variety of downhole and surface sensors were deployed to obtain sensitivity to a large bandwidth, including frequencies well below those that are typically monitored during a hydraulic fracture treatment. We observed high-frequency microseismic events to a maximum distance of ~ 1.6 km, and perforation shots to a distance of 2.0 km. Evidence is reported for delayed onset of high-frequency microseismic events associated with proppant injection. This behaviour may reflect less brittle response of the silty-shale Montney reservoir compared to other unconventional reservoirs in western Canada.

Various low-frequency microseismic signals are described and classified in this study. In some instances, low-frequency tremor

Broadband microseismic observations...

Continued from Page 51

signals appear as precursors to high-frequency microseismic events, suggesting a possible causal relationship. We interpret this type of low-frequency tremor activity to be an expression of deformation processes that are otherwise not seismically detectable. In addition, we observe very long-duration low-frequency tremor that persists throughout the treatment stages; this is interpreted to originate from coupling of pump-generated vibrations into the subsurface via the treatment wellbore. Differences between the low-frequency response observed here and previously documented long-period long-duration microseismic events from the Barnett shale are interpreted to reflect a lower degree of complexity in the pre-existing and induced fracture networks here.

Finally we observe some low-frequency signals that appear to be caused by natural earthquakes, unrelated to this fracture stimulation program and located ~ 150km from the study area. These events are not reported in the national earthquake catalog, likely because their magnitude falls below the detection threshold of existing seismograph stations used to monitor earthquakes. With much recent attention given to the potential for triggering of anomalous seismic events from hydraulic fracturing, it is very important to correctly identify and interpret such signals. *R*

References

Benson, P. M., S. Vinciguerra, P. G. Meredith, and R. P. Young, 2008, *Laboratory simulation of volcano seismicity:* Science, 322, 249–252.

Beroza, G.C. and Ide, S., 2011. *Slow Earthquakes and Nonvolcanic Tremor.* Annual Review of Earth and Planetary Sciences, 39: 271-296.

Boore, D. M. and Boatwright, J., 1984. *Average body- wave radiation coefficients,* Bull. Seism. Soc. Am., 74, 1615-1621.

Das, I. and Zoback, M., 2011. *Long Period Long Duration Seismic Events During Hydraulic Stimulation of a Shale Gas Reservoir.* The Leading Edge, July 2011 issue.

Dixon, J., 2000, *Regional lithostratigraphic units in the Triassic Montney Formation of western Canada:* Bulletin of Canadian Petroleum Geology, 40, 80-83

Edwards, D.E., Barclay, J.E., Gibson, D.W. Kvill,G.E. and Halton, E. 2008. *Triassic Strata of the Western Canada Sedimentary Basin. In, Geological Atlas of the Western Canada Sedimentary Basin.* Accessed online at http://www.ags.gov.ab.ca/publications/wcsb_atlas/a_ch16/ch_16.html on January 5, 2012.

Fisher, M. K., Wright, C. A., Davidson, B. M., Goodwin, A. K., Fielder, E. O., Buckler, W. S., and Steinsberger, N. P. (2005). *Integrating fracture-mapping technologies to improve stimulations in the Barnett Shale.* SPE Prod Fac, 20(2):doi:10.2118/77441–PA.

Maxwell, S., Urbancic, T., Steinsberger, N. and Zinno, R., 2002. *Microseismic Imaging of Hydraulic Fracture Complexity in the Barnett Shale.* SPE 77440-MS, doi: 10.2118/77440-MS.

National Energy Board (NEB), 2009. *Primer for Understanding Canadian Shale Gas.* Accessed online at http://www.neb.gc.ca/clf-nsi/rnrgynfmtn/nrgyrprt/ntrlgs/ prmrndrstndng-shlgs2009/ prmrndrstndngshlgs2009-eng.pdf on January 6, 2012.

Shelly, D.R., Beroza, G.C. and Ide, S., 2007. *Nonvolcanic tremor and low-frequency earthquake swarms.* Nature, 446: 305-307.

Thompson, B. D., R. P. Young, and D. A. Lockner, 2009, *Premonitory acoustic emissions and stick-slip in natural and smooth-faulted Westerly granite,* Journal of Geophysical Research, 114, B02205.

Walsh, W., Adams, C., Kerr, B., and Korol, J., 2006, *Regional "Shale Gas" Potential of the Triassic Doig and Montney Formations, Northeastern British Columbia:* British Columbia Ministry of Energy, Mines and Petroleum Resources, Petroleum Geology Open file 2006-02.

Broadband microseismic observations…

Dave Eaton received his B.Sc. from Queen's University in 1984 and M.Sc. and Ph.D. from the University of Calgary in 1988 and 1992. He rejoined the University of Calgary in 2007 after an 11-year academic career at the University of Western Ontario. His post-doctoral research experience included work at Arco's Research and Technical Services (Plano, Texas) and the Geological Survey of Canada (Ottawa). Besides microseismic, his current research is focused on the lithosphere-asthenosphere boundary. He is past-president of the Canadian Geophysical Union and Eastern Section of the Seismological Society of America, and a founding member of POLARIS, a $10 M infrastructure project funded by the Canada Foundation for Innovation (CFI). In 2008 he was awarded an $800K grant for CFI to support the development of a new earthquake monitoring network in Alberta and a unique microseismic monitoring system. He completed his 5-year term as Head of the Department of Geoscience in July 2012 and is currently on sabbatical. He was awarded a Benjamin Meaker Visiting Professorship from the University of Bristol, where he spent part of his sabbatical in Fall, 2012.
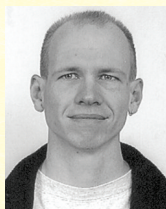
Mirko van der Baan graduated in 1996 from the University of Utrecht in the Netherlands, obtained a PhD with honors in 1999 from the Joseph Fourier University in Grenoble, France, and then joined the University of Leeds, UK, where he became the Reader of Exploration Seismology. He is currently an Associate Professors at the Department of Physics at the University of Alberta in 2008. He also holds an HDR (Habilitation) from University Denis Diderot, Paris, France. His research interests include attenuation and velocity anisotropy, signal processing, and microseismicity. He is currently an Associate Editor for Geophysics, serves on the SEG Research Committee, and a member of EAGE, CSEG and SEG.

Jean-Baptiste Tary is a post-doctoral fellow at the University of Alberta. He obtained a Ph.D. in marine geophysics in 2011 from the University of Western Brittany and Ifremer in France. His work, part of the Microseismic Industry Consortium project, consists in the study of the deformation of hydrocarbon reservoirs through the analysis of resonance frequencies and unconventional events occurring during hydraulic fracturing.

★ ★ ★ ★ ★ ★

November 13, 2012

CSEG Junior Geophysicists Forum
(Photo courtesy: Mohammed Al-Ibrahim.)

Junior
GEOPHYSICISTS
Forum